Response functions near the liquid-liquid critical point of ST2 water

Erik Lascaris[*], T. A. Kesselring[†], G. Franzese[**], S. V. Buldyrev[‡], H. J. Herrmann[†,§] and H. E. Stanley[*]

[*]*Center for Polymer Studies and Department of Physics, Boston University, Boston, MA 02215*
[†]*Computational Physics, IfB, ETH Zurich, Schafmattstrasse 6, 8093 Zurich, Switzerland*
[**]*Departament de Física Fonamental, Universitat de Barcelona, Diagonal 645, 08028 Barcelona, Spain*
[‡]*Department of Physics, Yeshiva University, 500 West 185th Street, New York, NY 10033*
[§]*Departamento de Física, Universidade Federal do Ceará, Campus do Pici, 60451-970 Fortaleza, Ceará, Brazil*

Abstract. We simulate the ST2 water model for time periods up to 1000 ns, and for four different system sizes, $N = 6^3$, 7^3, 8^3, and 9^3. We locate the liquid-liquid phase transition line and its critical point in the supercooled region. Near the liquid-liquid phase transition line, we observe that the system continuously flips between the low-density and high-density liquid phases. We analyze the transition line further by calculating two thermodynamic response functions, the isobaric specific heat capacity C_P and the isothermal compressibility K_T. We use two different methods: (i) from fluctuations and (ii) with the relevant thermodynamic derivative. We find that, within the accuracy of our simulations, the maxima of two different response functions occur at the same temperatures. The lines of C_P and K_T maxima below the critical pressure approximate the Widom line which is continuous with the line of first-order transitions in the two-phase region where we observe the phase flipping.

Keywords: water, liquid-liquid critical point, response functions, molecular dynamics
PACS: 61.20.Ja, 61.20.Gy

INTRODUCTION

According to the liquid-liquid critical point (LLCP) hypothesis [1] there exists a second critical point in the metastable supercooled region of the phase diagram of liquid water. This LLCP would explain the unusually steep increase that the thermodynamic response functions display when water is supercooled to temperatures far below the melting temperature [2, 3, 4, 5, 6, 7, 8, 9], and a range of dynamical anomalies [10, 11, 12]. It would be consistent with dynamical anomalies [13, 14, 15, 16, 17] studied in experiments [18, 19, 20] and it would explain a very low-temperature dynamical crossover observed in water hydrating protein [21, 22]. It would also clarify the existence of the two distinct amorphous solid phases LDA and HDA that have been experimentally observed by quenching water to temperatures near 77 K at different pressures [23, 24, 25]. The LLCP hypothesis states that at such low temperatures there exist two different liquid phases: (i) a low-density liquid (LDL) that can vitrify to become low-density amorphous ice (LDA) as the temperature is lowered further, and (ii) a high-density liquid (HDL) that can vitrify into high-density amorphous ice (HDA). Alternative hypotheses and their relation with the LLCP scenario have been discussed in Ref. [26].

Although the LLCP hypothesis was introduced over twenty years ago, and its occurrence in other fluid has strong experimental evidences (see [27] for a recent review) the existence and location of the critical point and the associated first-order phase transition line for water are still a subject of hot debate. Even though a large number of experiments are consistent with the LLCP hypothesis [28, 29, 30, 31], results from simulation are less clear [32, 33, 34, 35, 36, 37, 38, 39, 40, 41, 42]. One reason for this is that as supercooled water is cooled to lower and lower temperatures it becomes more and more susceptible to crystallization, until at the pressure-dependent homogeneous nucleation temperature T_H (e.g., $T_H \simeq -38^\circ$C at 1 atm) crystallization occurs too quickly for the LLCP to be witnessed in most experiments. Crystallization is not a problem for computer simulations, however, as they can explore much smaller time scales.

Heating up the glassy states LDA and HDA leads to spontaneous crystallization at a temperature $T_X < T_H$ (e.g., $T_X \simeq -123^\circ$C at 1 atm) and therefore the region of the phase diagram between T_H and T_X is not accessible experimentally, even though water can be expected to be a metastable liquid on a sufficiently short time scale. This region, $T_X < T < T_H$, is often referred to as the "no man's land" of liquid water.

4th International Symposium on Slow Dynamics in Complex Systems
AIP Conf. Proc. 1518, 520-526 (2013); doi: 10.1063/1.4794628

MODEL

A popular model for simulations of supercooled water is the ST2 model [43], because it has a relatively large self-diffusion compared to other water models, which means it suffers less from the extremely slow dynamics that occur at the low temperatures of interest here.

Introduced by Stillinger and Rahman in 1974, the ST2 model represents a water molecule by a rigid structure of five particles that is shaped like a tetrahedron. In its center there is a neutral oxygen atom, surrounded by two positively charged particles that represent the hydrogen atoms, and two negative particles that represent the lone pair electrons. The oxygen atoms interact via a Lennard-Jones potential, while the charged particles interact with each other via the Coulomb potential.

In the ST2 model the short-range electrostatics drops to zero by means of a smoothing function. For the long-range part of the electrostatic interaction the original model used a simple cutoff which nowadays is known to produce artifacts. We therefore use here the more sophisticated reaction field method as described in [44].

PHASE DIAGRAM

We perform 624 molecular dynamics (MD) simulations at constant pressure and temperature (the *NPT* ensemble) for times up to 1μs and for four system sizes $N = 6^3$, 7^3, 8^3, and 9^3. In all our simulations we use the Berendsen barostat and a Nosé-Hoover thermostat, and equilibrate the system for at least 100 ns before each production run. The results are summarized in Fig. 1. We demonstrate the existence of (i) two supercooled liquids, LDL and HDL, (ii) the liquid-liquid phase transition (LLPT) line that separates them, and (iii) the LLCP. In [39] it was estimated that the LLCP is located approximately at $T_C = 246$ K and $P_C = 208$ MPa, indicated in Fig. 1 as the white area labeled LLCP. Within the purple region of Fig. 1 we find that the system continuously flips between the LDL and HDL phase. This phase flipping is clearly visible in the *NPT* ensemble by considering the evolution of the density (see Fig. 2). Above the critical pressure P_C this coexistence region represents the location of the LLPT. However, because of finite size effects the flipping also occurs at pressures below P_C, on a line known as the Widom line [45, 46]. The Widom line is defined as the loci of correlation length maxima, or as the line where the maxima of different response functions come together as they approach the critical point [46, 47].

RESPONSE FUNCTIONS

To show the existence of a LLPT line in the thermodynamic limit a detailed finite-size scaling analysis has been performed by Kesselring *et al.* [39] following standard methods that have been described in previous publications [48, 49, 50, 51, 52, 53]. Here, we limit the discussion to the case of a fixed finite size $N = 343$, for which several evidences can be given for the occurrence of a LLPT. One is the flipping in Fig. 2 between two coexisting phases with different densities. As LDL and HDL have different structures, the LLPT can also be witnessed by looking at the intermediate scattering function $S(k)$ or the radial distribution function $g(r)$, which display an abrupt change at the LLPT line.

A very direct way to look at the LLPT and its associated critical point is by considering response functions such as the constant pressure specific heat

$$C_P \equiv \left(\frac{\partial \langle H \rangle}{\partial T} \right)_P \tag{1}$$

and the isothermal compressibility

$$K_T \equiv -\frac{1}{\langle V \rangle} \left(\frac{\partial \langle V \rangle}{\partial P} \right)_T . \tag{2}$$

In Fig. 3a we plot the average enthalpy $\langle H \rangle$ for each state point, and we introduce the following fit

$$\langle H(T) \rangle = a_1 + a_2 \, \mathrm{erf}[a_3 (T - a_4)] \tag{3}$$

where a_i with $i = 1, \ldots, 4$ are fitting parameters. The derivative of this fitting formula results in a Gaussian approximation to $\partial \langle H \rangle / \partial T$, shown in Fig. 3b together with the centered difference of the original data.

The specific heat can also be calculated from enthalpy fluctuations. In the isothermal-isobaric ensemble a thermostat forces the temperature to remain close to T_0, while a barostat keeps the average pressure near P_0. The specific heat is then related to the instantaneous enthalpy $H = E_{\mathrm{tot}} + P_0 V$ through

$$k_B T_0^2 C_P = \langle H^2 \rangle - \langle H \rangle^2 \tag{4}$$

where k_B is the Boltzmann constant. The result of this calculation is shown in Fig. 3c together with the C_P calculated via the derivative.

As with the heat capacity, also the isothermal compressibility K_T can be calculated with two different methods: using its definition Eq. (2), or via fluctuations. The results of each methods are compared in Fig. 3d. The isothermal compressibility K_T is related to volume fluctuations according to

$$\langle V \rangle k_B T_0 K_T = \langle V^2 \rangle - \langle V \rangle^2 \tag{5}$$

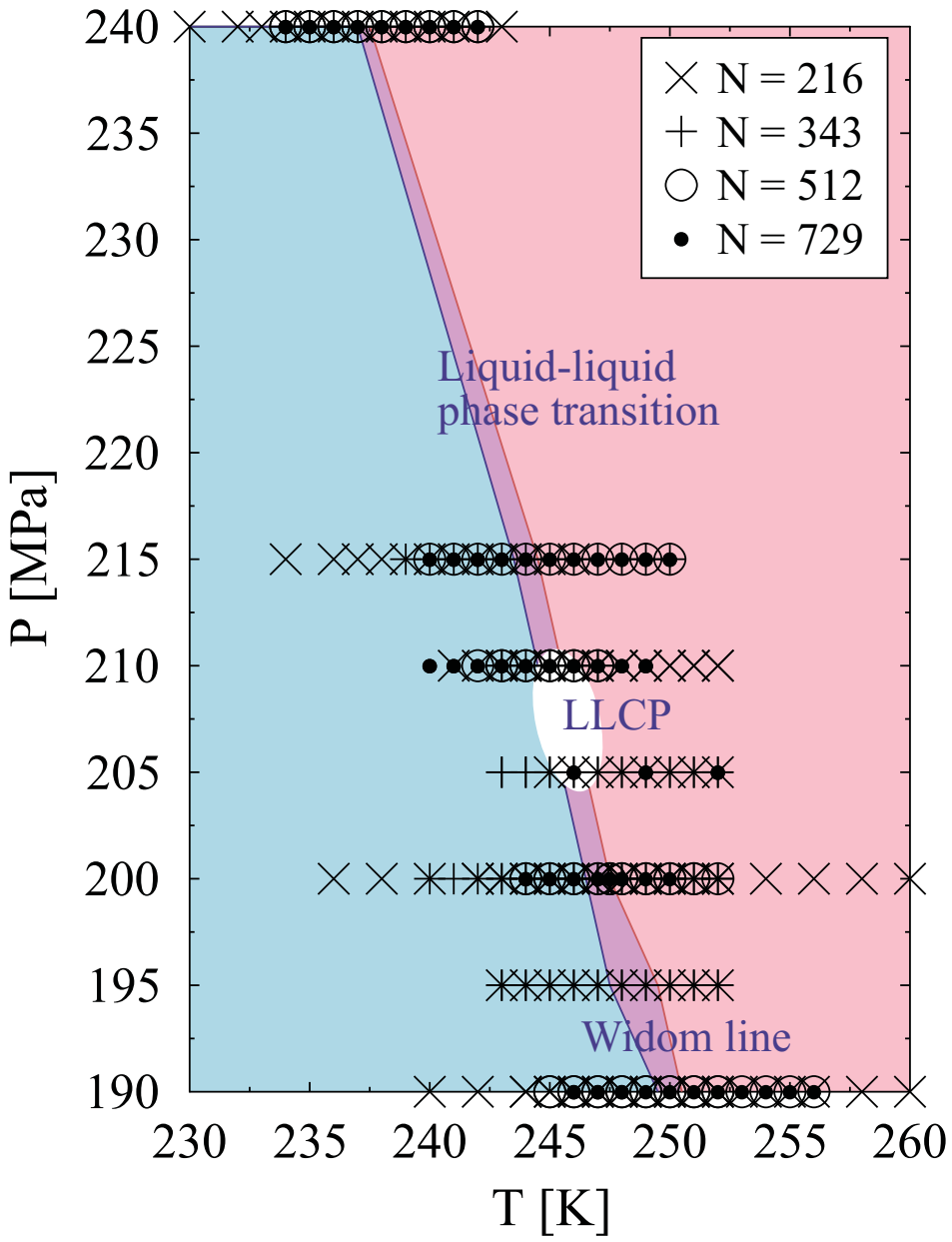

FIGURE 1. Overview of the simulations that have been performed, with the symbols indicating the four different system sizes $N = 216$, 343, 512, and 729 molecules. The high-T (pink) region exhibits HDL-like states and the low-T (blue) region the LDL-like states. In the intermediate (purple) region we observe flipping between HDL-like and LDL-like states. The white region, denoted LLCP, is our estimate of the location of the liquid-liquid critical point. The purple region for pressures above the LLCP is an estimate of the liquid-liquid phase transition line, while below the LLCP the purple region encloses the Widom line.

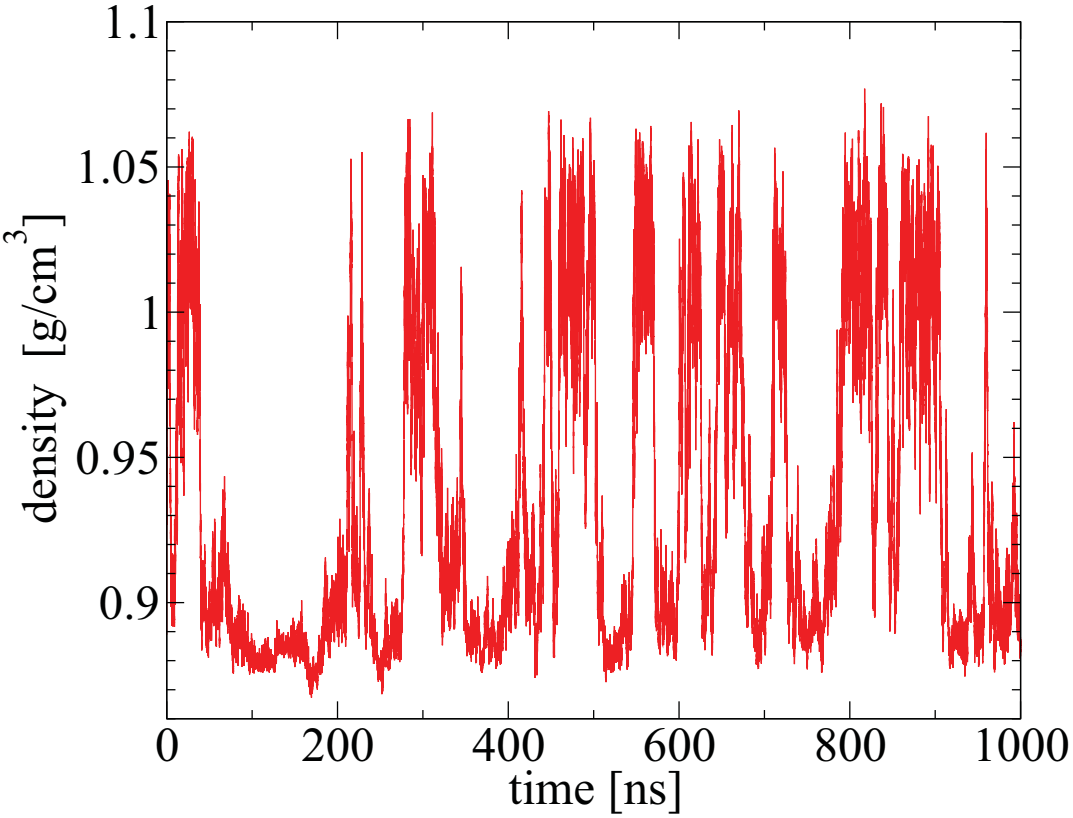

FIGURE 2. Phase flipping between the LDL and HDL phases at the coexistence line, at constant $P = 215$ MPa and $T = 244$ K for $N = 343$ ST2 molecules. The 1000 ns time series shows how frequently the system switches from LDL to HDL states. For the LDL phase $\rho \approx (0.89 \pm 0.01)$ g/cm^3 and for the HDL phase $\rho \approx (1.02 \pm 0.03)$ g/cm^3, corresponding to a difference of about 15% in density.

where $\langle V \rangle$ is the average volume, and T_0 the temperature set by the thermostat. Calculating K_T via its definition requires calculating $\langle \ln(V) \rangle$ as function of P_0 and then taking the derivative. Since we only have simulations for a few different pressures we do not obtain a very good estimate for K_T via this method.

DISCUSSION AND CONCLUSIONS

The calculations of the response functions with different methods produce remarkably similar results for C_P. In particular, the height and location of the specific heat maxima are in excellent agreement for the three methods adopted here (Fig. 3b,c). This comparison shows that our MD simulations in the *NPT* ensemble are well equilibrated and that the fluctuations are well calculated.

For a first-order phase transition, one would expect the response functions to diverge at the LLCP. Finite size effects prevent this from occurring. However, the size we consider here for the calculation of the response functions ($N = 343$) is large enough to find that the maxima of both C_P and K_T fall within the phase flipping region of Fig. 1, as shown in Fig. 4.

In conclusion, the response function calculation reported here, together with the finite-size scaling analysis of Ref. [39] and the detailed analysis of the characteristic relaxation times compared to the crystal nucleation times in the conditions considered here, demonstrate the occurrence in the supercooled region of ST2 water, metastable with respect to the crystal phase, of a genuine LLPT between two liquid phases, with different densities and with structures, that differ mainly at the second coordination shell [54] (see also similar consideration for a different system in [55]).

ACKNOWLEDGMENTS

We thank Y. Liu, A. Z. Panagiotopoulos, P. Debenedetti, F. Sciortino, I. Saika-Voivod and P. H. Poole for sharing their results, obtained using approaches different from ours, but also addressing the LLCP hypothesis. GF thanks Spanish MEC grant FIS2012-31025 and EU

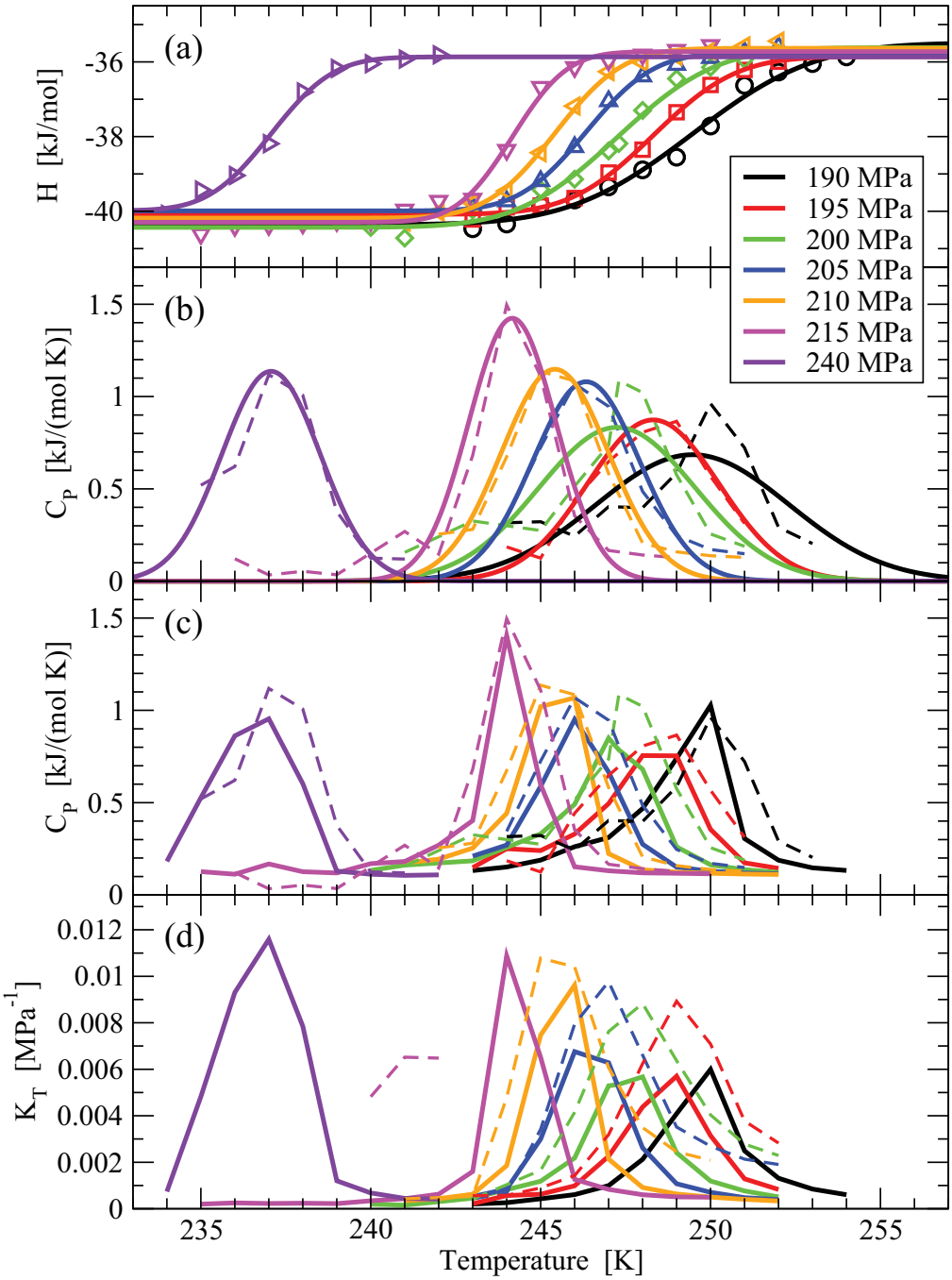

FIGURE 3. Calculation of the response functions C_P and K_T near the liquid-liquid critical point of ST2 from our MD simulations for $N = 343$. In all the panels curves correspond to different pressures, going from $P = 190$ MPa (rightmost curve) to $P = 240$ MPa (leftmost curve). (a) Average enthalpy vs. temperature for different pressures. Symbols are averages from our MD simulations. Solid curves indicate fits to Eq. 3. (b) The constant pressure specific heat $C_P = \partial H/\partial T$ from the derivatives of the fitting curves in (a) (shown as continuous lines) and from the centered differences of the simulation data points (shown as dashed lines). (c) The good comparison between C_P calculated from enthalpy fluctuations (solid curves) and C_P calculated by centered differences of enthalpy as in panel (b) (dashed curves) shows that our MD simulations are well equilibrated. (d) The comparison between the isothermal compressibility K_T calculated from volume fluctuations (solid curves) and K_T calculated via its definition Eq. 2 (dashed curves), shows a lesser quality than the case in panel (c) due to the small number of isobars simulated.

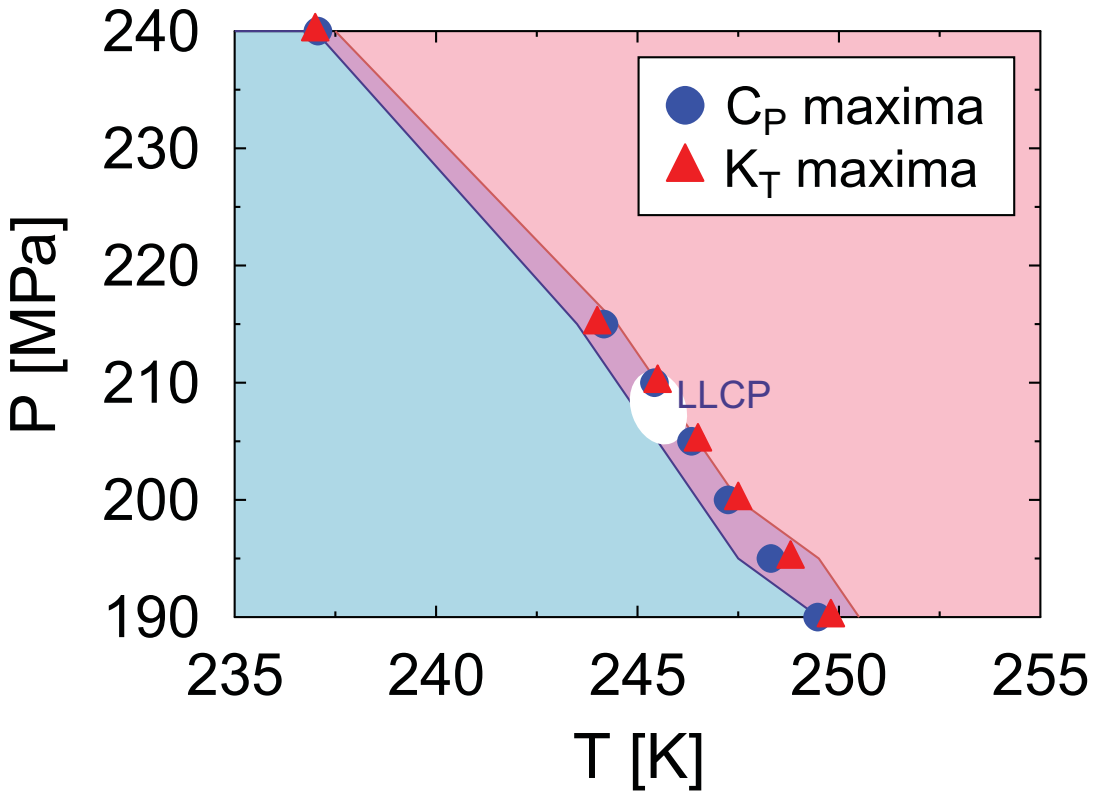

FIGURE 4. Maxima of the response functions, extracted from Fig. 3c and Fig. 3d and superposed onto the phase diagram of Fig. 1. This shows that the phase transition line (and the Widom line) indeed coincide with the phase flipping and the maxima of the response functions.

FP7 grant NMP4-SL-2011-266737 for support. SVB acknowledges the partial support of this research through the Dr. Bernard W. Gamson Computational Science Center at Yeshiva College and through the Departament d'Universitats, Recerca i Societat de la Informació de la Generalitat de Catalunya. HES thanks the NSF Chemistry Division for support (grants CHE 0911389 and CHE 0908218). HJH thanks the European Research Council (ERC) Advanced Grant 319968-FlowCCS.

REFERENCES

1. P. H. Poole, F. Sciortino, U. Essmann, and H. E. Stanley, *Nature* **360**, 324–328 (1992).
2. C. A. Angell, J. Shuppert, and J. C. Tucker, *J. Phys. Chem.* **77**, 3092–3099 (1973).
3. R. J. Speedy, and C. A. Angell, *J. Chem. Phys.* **65**, 851–858 (1976).
4. C. A. Angell, W. J. Sichina, and M. Oguni, *J. Phys. Chem.* **86**, 998–1002 (1982).
5. R. J. Speedy, *J. Phys. Chem.* **86**, 982–991 (1982).
6. V. Holten, C. E. Bertrand, M. A. Anisimov, and J. V. Sengers, *J. Chem. Phys.* **136**, 094507 (2012).
7. V. Holten, J. Kalová, M. A. Anisimov, and J. V. Sengers, *Int. J. Thermophys.* **33**, 758–773 (2012).
8. C. E. Bertrand, and M. A. Anisimov, *J. Phys. Chem. B* **115**, 14099–14112 (2011).
9. M. G. Mazza, K. Stokely, H. E. Stanley, and G. Franzese, *J. Chem. Phys.* **137**, 204502 (2012).
10. P. Kumar, and H. E. Stanley, *J. Phys. Chem. B* **115**, 14269–14273 (2011).
11. F. Sciortino, P. H. Poole, H. E. Stanley, and S. Havlin, *Phys. Rev. Lett.* **64**, 1686–1689 (1990).
12. F. W. Starr, J. K. Nielsen, and H. E. Stanley, *Phys. Rev. Lett.* **82**, 2294–2297 (1999).
13. P. Kumar, G. Franzese, and H. E. Stanley, *Phys. Rev. Lett.* **100**, 105701 (2008).
14. P. Kumar, G. Franzese, and H. E. Stanley, *J. Phys.: Condens. Matter* **20**, 244114 (2008).
15. G. Franzese, and F. de los Santos, *J. Phys.: Condens. Matter* **21**, 504107 (2009).
16. F. de los Santos, and G. Franzese, *J. Phys. Chem. B* **115**, 14311–14320 (2011).
17. F. de los Santos, and G. Franzese, *Phys. Rev. E* **85**, 010602 (2012).
18. G. Franzese, K. Stokely, X. Q. Chu, P. Kumar, M. G.

Mazza, S. H. Chen, and H. E. Stanley, *J. Phys.: Condens. Matter* **20**, 494210 (2008).
19. H. E. Stanley, P. Kumar, S. Han, M. G. Mazza, K. Stokely, S. V. Buldyrev, G. Franzese, F. Mallamace, and L. Xu, *J. Phys.: Condens. Matter* **21**, 504105 (2009).
20. H. E. Stanley, S. V. Buldyrev, G. Franzese, P. Kumar, F. Mallamace, M. G. Mazza, K. Stokely, and L. Xu, *J. Phys.: Condens. Matter* **22**, 284101 (2010).
21. P. Kumar, Z. Yan, L. Xu, M. G. Mazza, S. V. Buldyrev, S.-H. Chen, S. Sastry, and H. E. Stanley, *Phys. Rev. Lett.* **97**, 177802 (2006).
22. M. G. Mazza, K. Stokely, S. E. Pagnotta, F. Bruni, H. E. Stanley, and G. Franzese, *Proc. Natl. Acad. Sci. U.S.A.* **108**, 19873–19878 (2011).
23. O. Mishima, L. D. Calvert, and E. Whalley, *Nature* **310**, 393–395 (1984).
24. O. Mishima, L. D. Calvert, and E. Whalley, *Nature* **314**, 76–78 (1985).
25. L. Xu, N. Giovambattista, S. V. Buldyrev, P. G. Debenedetti, and H. E. Stanley, *J. Chem. Phys.* **134**, 064507 (2011).
26. K. Stokely, M. G. Mazza, H. E. Stanley, and G. Franzese, *Proc. Natl. Acad. Sci. U.S.A.* **107**, 1301–1306 (2010).
27. P. Vilaseca, and G. Franzese, *J. Non-Cryst. Solids* **357**, 419–426 (2011).
28. O. Mishima, *J. Chem. Phys.* **100**, 5910–5912 (1994).
29. O. Mishima, and H. E. Stanley, *Nature* **392**, 164–168 (1998).
30. O. Mishima, and H. E. Stanley, *Nature* **396**, 329–335 (1998).
31. M. Beye, F. Sorgenfrei, W. F. Schlotter, W. Wurth, and A. Föhlisch, *Proc. Natl. Acad. Sci. U.S.A.* **107**, 16772–16776 (2010).
32. S. Harrington, P. H. Poole, F. Sciortino, and H. E. Stanley, *J. Chem. Phys.* **107**, 7443–7450 (1997).
33. P. H. Poole, I. Saika-Voivod, and F. Sciortino, *J. Phys.: Condens. Matter* **17**, L431–L437 (2005).
34. Y. Liu, A. Z. Panagiotopoulos, and P. G. Debenedetti, *J. Chem. Phys.* **131**, 104508 (2009).
35. Y. Liu, A. Z. Panagiotopoulos, and P. G. Debenedetti, *J. Chem. Phys.* **132**, 144107 (2010).
36. D. T. Limmer, and D. Chandler, *J. Chem. Phys.* **135**, 134503 (2011).
37. F. Sciortino, I. Saika-Voivod, and P. H. Poole, *Phys. Chem. Chem. Phys.* **13**, 19759–19764 (2011).
38. P. H. Poole, S. R. Becker, F. Sciortino, and F. W. Starr, *J. Phys. Chem. B* **115**, 14176–14183 (2011).
39. T. A. Kesselring, G. Franzese, S. V. Buldyrev, H. J. Herrmann, and H. E. Stanley, *Sci. Rep.* **2**, 474 (2012).
40. P. Gallo, and F. Sciortino, *Phys. Rev. Lett.* **109**, 177801 (2012).
41. Y. Liu, J. C. Palmer, A. Z. Panagiotopoulos, and P. G. Debenedetti, *J. Chem. Phys.* **137**, 214505 (2012).
42. P. H. Poole, R. K. Bowles, I. Saika-Voivod, and F. Sciortino, *J. Chem. Phys.* **138**, 034505 (2013).
43. F. H. Stillinger, and A. Rahman, *J. Chem. Phys.* **60**, 1545–1557 (1974).
44. O. Steinhauser, *Mol. Phys.* **45**, 335–348 (1982).
45. L. Xu, P. Kumar, S. V. Buldyrev, S.-H. Chen, P. H. Poole, F. Sciortino, and H. E. Stanley, *Proc. Natl. Acad. Sci. U.S.A.* **102**, 16558–16562 (2005).
46. G. Franzese, and H. E. Stanley, *J. Phys.: Condens. Matter* **19**, 205126 (2007).
47. Y. Zhang, A. Faraone, W. A. Kamitakahara, K.-H. Liu, C.-Y. Mou, J. B. Leão, S. Chang, and S.-H. Chen, *Proc. Natl. Acad. Sci. U.S.A.* **108**, 12206–12211 (2011).
48. G. Franzese, and A. Coniglio, *Phys. Rev. E* **58**, 2753–2759 (1998).
49. G. Franzese, V. Cataudella, S. E. Korshunov, and R. Fazio, *Phys. Rev. B* **62**, R9287–R9290 (2000).
50. G. Franzese, *Phys. Rev. E* **61**, 6383–6391 (2000).
51. G. Franzese, A. Hernando-Martínez, P. Kumar, M. G. Mazza, K. Stokely, E. G. Strekalova, F. de los Santos, and H. E. Stanley, *J. Phys.: Condens. Matter* **22**, 284103 (2010).
52. E. G. Strekalova, M. G. Mazza, H. E. Stanley, and G. Franzese, *Phys. Rev. Lett.* **106**, 145701 (2011).
53. E. G. Strekalova, M. G. Mazza, H. E. Stanley, and G. Franzese, *J. Phys.: Condens. Matter* **24**, 064111 (2012).
54. T. A. Kesselring, E. Lascaris, G. Franzese, S. V. Buldyrev, H. J. Herrmann, and H. E. Stanley, *arXiv:cond-mat* (2013), `1302.1894`.
55. P. Vilaseca, and G. Franzese, *J. Chem. Phys.* **133**, 084507 (2010).